Geochronology and Paleoenvironmental Changes of Late Pleistocene Sediments in the Ross Sea, Antarctica

Guogang Li[1], Ruyuan Bu[1]*, Liang Yi[2]*, Bangqi Hu[3], Yunhai Li[4], Youjun Ji[5], Yixin Li[1] and Liang Wang[4]

[1]North China Sea Administration, Ministry of Natural Resources, Qingdao, China, [2]Laboratory of Marine Geology, Tongji University, Shanghai, China, [3]Qingdao Institute of Marine Geology, China Geological Survey, Qingdao, China, [4]Third Institute of Oceanography, Ministry of Natural Resources, Xiamen, China, [5]Second Institute of Oceanography, Ministry of Natural Resources, Hangzhou, China

The palaeoceanographic studies are largely limited by poor carbonate preservation in high-latitude regions. To improve our knowledge in this key area, we studied a sediment core (ANT32-RA05C) in terms of paleomagnetic and ^{230}Th dating and geochemical properties, collected from the continental slope of the Ross Sea, Antarctica. The two major results are as follows: 1) the sedimentation rate based on ^{230}Th isotopes is 1.37 cm/kyr, agreeing well with the correlation of the relative paleomagnetic intensity of the core ANT32-RA05C to changes in Earth's magnetic intensity and 2) the sediments contain ice-rafted debris (IRD) over 30%, with a considerable contribution of siliceous deposits. Integrating geochronological and geochemical properties of the studied core, a correlation of the regional paleoenvironmental process to the EPICA Dome C (EDC) Antarctic temperature is established, inferring that the IRD input and primary productivity are both enhanced in a warm climate. Moreover, a leading phase of biogenic processes to changes in the ice sheet in the Ross Ice Shelf is observed, highlighting a dominant role of the oceanic circulation in the ice-sheet retreat during the last deglaciation. Overall, the sedimentary record in the Ross Sea documents some key features of the paleoenvironmental processes in the Late Pleistocene, which could be correlated with large-scale changes in Antarctica and thus are worthy of further investigation in the future.

Keywords: Ross Sea, Late Pleistocene, paleomagnetism, ^{230}Th dating, ice-rafted debris, biogenic silica

INTRODUCTION

The Ross Sea with the Ross Ice Shelf is the second largest bay in Antarctica and has the largest ice shelf on Earth, whose size is extremely sensitive to the global climatic change (Mckay et al., 2008; Wilson et al., 2012; Brachfeld et al., 2013; Rignot et al., 2013; Ohneiser et al., 2019). Because of this, climate change and environmental evolution in the Ross Sea attracted great attention in the past decades, such as palaeoceanographic, glacial (ice sheets/sea ice), and climatic processes since the late Quaternary (Domack et al., 1999; Shipp et al., 1999; Bart and Cone, 2012; Anderson et al., 2014; Yokoyama et al., 2016). For example, Domack et al. (1999) and Mckay et al. (2008) studied the sediments from till to glacimarine and identified a progressive retreat of the ice shelf during the last deglaciation. Mosola and Anderson (2006) investigated several cores including terrigenous glacimarine sediments from the eastern Ross Sea and found that the absence of the upper

FIGURE 1 | Schematic map of the study area. The red star represents the core ANT32-RA05C in this study, and the yellow dots represent the cores nearby the study area. EDC, EPICA Dome C ice core (Jouzel et al., 2007); WLK, Wilkes Land Basin cores (Macrì et al., 2005); and Eltanin, Eltanin cores (Jovane et al., 2008). Oceanic circulation was modified from Carter et al. (2008), Dotto et al. (2018); Cook et al. (2017), and Li et al. (2021).

diatomaceous facies could be attributed to the sea-ice cover. Based on the ice-rafted debris (IRD) records, Li et al. (2021) investigated changes in the ice shelf and the iceberg discharge since the marine isotope stage (MIS) 13 and reported a shift in the terrigenous sources.

Because of the limited dating materials and large uncertainties in dating organic carbon (Sikes et al., 2000; Pugh et al., 2009; Skinner et al., 2010; Xiao et al., 2016), chronological works based on AMS ^{14}C dating and oxygen isotope stratigraphy are usually not suitable in such high-latitude regions, causing lots of unknowns of the past changes in the sedimentary and palaeoceanographic processes in the Ross Sea. Recently, several comprehensive records of the relative paleomagnetic intensity (RPI) have been established (Guyodo and Valet, 1999; Sagnotti et al., 2001; Stoner et al., 2002; Macrì et al., 2005; Jovane et al., 2008; Channell et al., 2009; Lisé-Pronovost et al., 2013), providing an opportunity to precise the dating of sediments without carbonate materials, and this method has been successfully applied in various paleoenvironmental studies in the Southern Ocean (Sagnotti et al., 2001; Branchfeld et al., 2003; Macrì et al., 2005; Macrì et al., 2006; Collins et al., 2012; Xiao et al., 2016). Therefore, in this study, based on the sediment core ANT32-RA05C from the continental slope of the Ross Sea, paleomagnetic and [230]Th dating are used to determine the age model, and the geochemical properties are carried out to provide a reconstruction of the climatic and oceanic evolution in the Ross Sea since the Late Pleistocene.

REGIONAL SETTING

The Ross Sea is a marginal sea, with the Victoria Land to the west and the Marie Byrd Land to the east (**Figure 1**). The Ross Sea Shelf has a typical glacial topography shaped by ice streams (Mosola and Anderson, 2006; Anderson et al., 2014), with an average depth of ~530 m and rapidly increasing to 3000 m in the shelf margin (Smith et al., 2012). In cold seasons (from March to November), the Ross Sea Shelf is generally frozen, and the sea ice extends to the outer region near 60°S, while in warm seasons (December to February), the sea ice melts and most of the bedrocks nearshore are exposed (Anderson et al., 2014). The oceanic circulation in the Ross Sea is mainly composed of the Antarctic Circumpolar Current driven by the westerly winds, the Antarctic Slope Current driven by the polar easterly winds, and the clockwise Ross Gyre sandwiched between them (Carter et al., 2008; Dotto et al., 2018; Li et al., 2021).

The melting process of the Ross Ice Shelf is characterized by the collapse and detachment of icebergs and large ice masses, which are driven by the ocean currents and surface winds that unload large amounts of ice-rafted debris onto the continental shelf and open ocean. Since the Late Pleistocene, the Ross Ice Shelf expanded and retreated several times (Naish et al., 2009), and the grounding line migrated northward further onto the Ross Sea Shelf in the Last Glacial Maximum (LGM) (Domack et al., 1999; Shipp et al., 1999; Anderson et al., 2014).
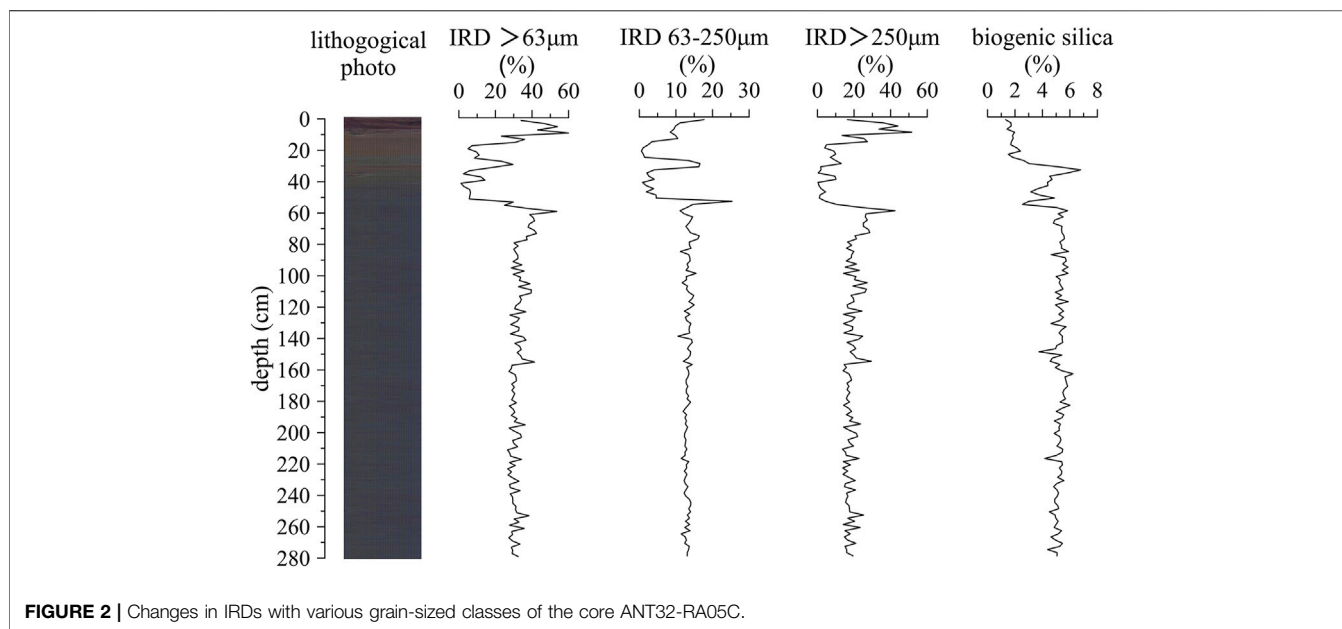
FIGURE 2 | Changes in IRDs with various grain-sized classes of the core ANT32-RA05C.
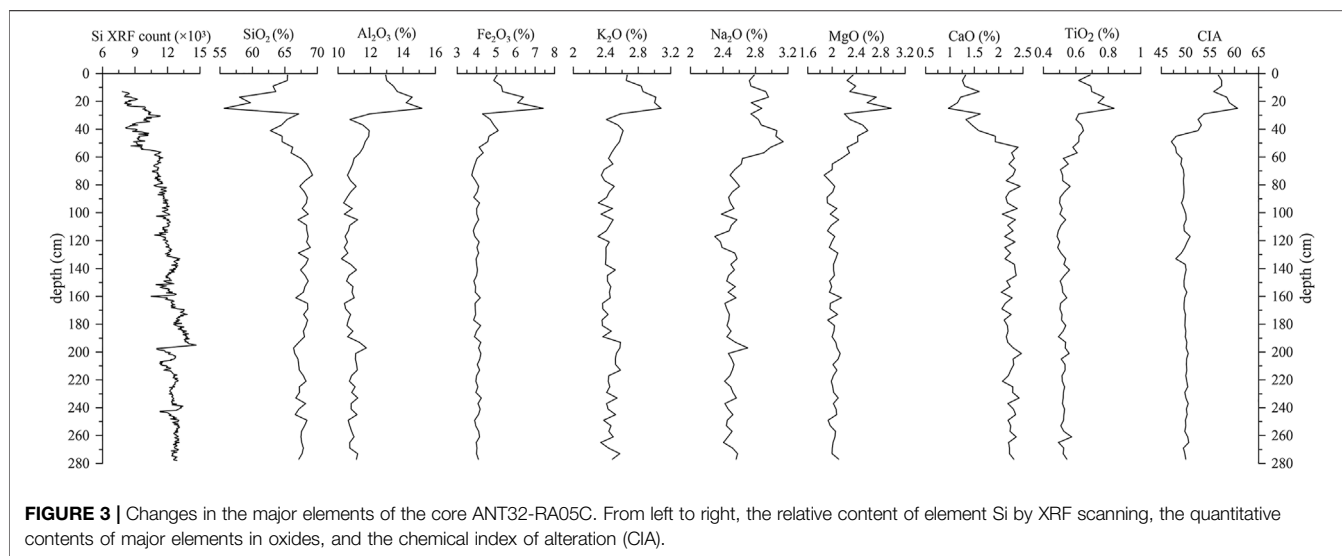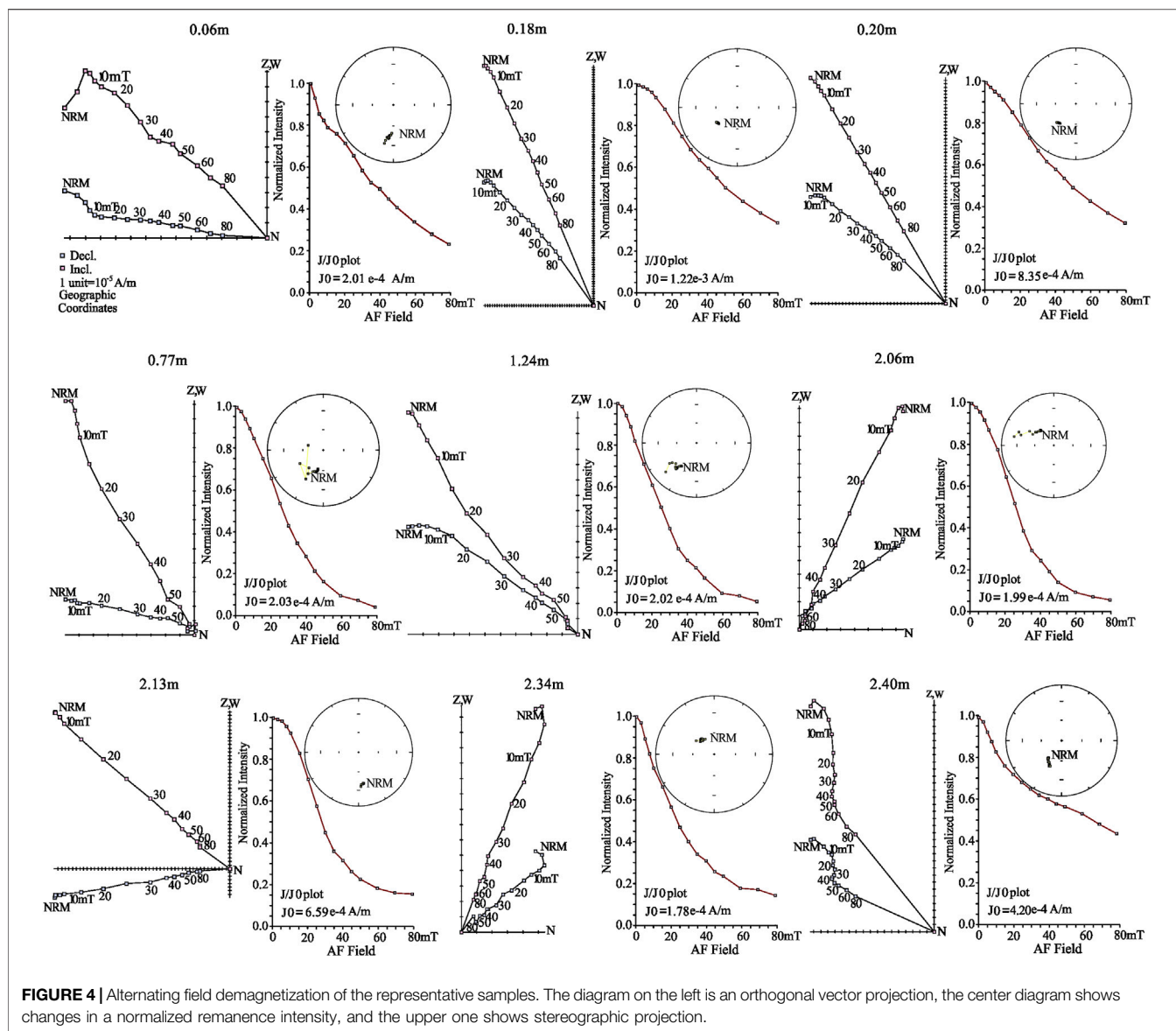

FIGURE 3 | Changes in the major elements of the core ANT32-RA05C. From left to right, the relative content of element Si by XRF scanning, the quantitative contents of major elements in oxides, and the chemical index of alteration (CIA).

TABLE 1 | Pearson correlation matrix of major elements, biogenic silica (BSi), and IRD contents in the core sediments.

	SiO$_2$	Al$_2$O$_3$	CaO	Fe$_2$O$_3$	K$_2$O	MgO	MnO	Na$_2$O	P$_2$O$_5$	TiO$_2$	BSi
Al$_2$O$_3$	−0.925	—	—	—	—	—	—	—	—	—	—
CaO	0.755	−0.789	—	—	—	—	—	—	—	—	—
Fe$_2$O$_3$	−0.972	0.930	−0.845	—	—	—	—	—	—	—	—
K$_2$O	−0.912	0.976	−0.715	0.903	—	—	—	—	—	—	—
MgO	−0.951	0.857	−0.779	0.925	0.831	—	—	—	—	—	—
MnO	−0.463	0.629	−0.665	0.527	0.569	0.431	—	—	—	—	—
Na$_2$O	−0.716	0.673	−0.588	0.644	0.640	0.811	0.338	—	—	—	—
P$_2$O$_5$	−0.762	0.754	−0.633	0.759	0.703	0.763	0.414	0.717	—	—	—
TiO$_2$	−0.935	0.940	−0.832	0.947	0.906	0.926	0.574	0.771	0.814	—	—
BSi	0.719	−0.872	0.712	−0.754	−0.808	−0.701	−0.675	−0.611	−0.678	−0.813	—
IRD	0.534	−0.279	0.366	−0.465	−0.314	−0.578	0.263	−0.502	−0.310	−0.403	0.084

N=70, bold numbers are significant at p < 0.01 level, and italics are significant at p < 0.05.

FIGURE 4 | Alternating field demagnetization of the representative samples. The diagram on the left is an orthogonal vector projection, the center diagram shows changes in a normalized remanence intensity, and the upper one shows stereographic projection.

MATERIALS AND METHODS

The sediment core ANT32-RA05C (176.02°W, 74.95°S, 1878 m water depth) was collected in the central continental slope of the Ross Sea, during the 32nd Chinese Antarctic Research Expedition (**Figure 1**). The length of the core is 280 cm and was cut and scanned after photographing and description by X-ray fluorescence (XRF) with a scanning interval of 0.5 cm.

For paleomagnetic dating, the samples were collected from the core using the U-channel tubes (2 cm × 2 cm × 150 cm), which were then subjected to alternating field (AF) demagnetization up to 90 mT. Magnetic susceptibility (MS) was measured using a Bartington MS2 meter. Anhysteretic remanent magnetization (ARM) was imparted to the samples using a peak AF of 100 mT and a direct biasing field of 0.05 mT using a 2G Enterprises SQUID magnetometer with inline AF coils. The

isothermal remanent magnetization was produced with a 2G Enterprises model 660 pulse magnetizer successively in the pulsed fields of 1 T (saturated isothermal remanent magnetization, SIRM) and −0.3 T (IRM$_{300mT}$) fields. All the magnetic measurements were conducted at the Institute of Earth Environment, Chinese Academy of Sciences.

For the IRDs, major elements, and biogenic silica content, the core was sampled for each 2 cm, and 140 subsamples in total were obtained. The procedure for the IRDs is as follows: after removing the organic matter with H_2O_2, it was sieved through a 63 μm standard sieve. The dried residuals were then shifted through a standard sieve of 250 μm. The biogenic silica in the sediments was extracted by sodium carbonate solution and reacted with ammonium molybdate to generate silico-molybdenum yellow, which was measured by using a spectrophotometer (Unico UV2802PC) in the Laboratory of Element and Isotope
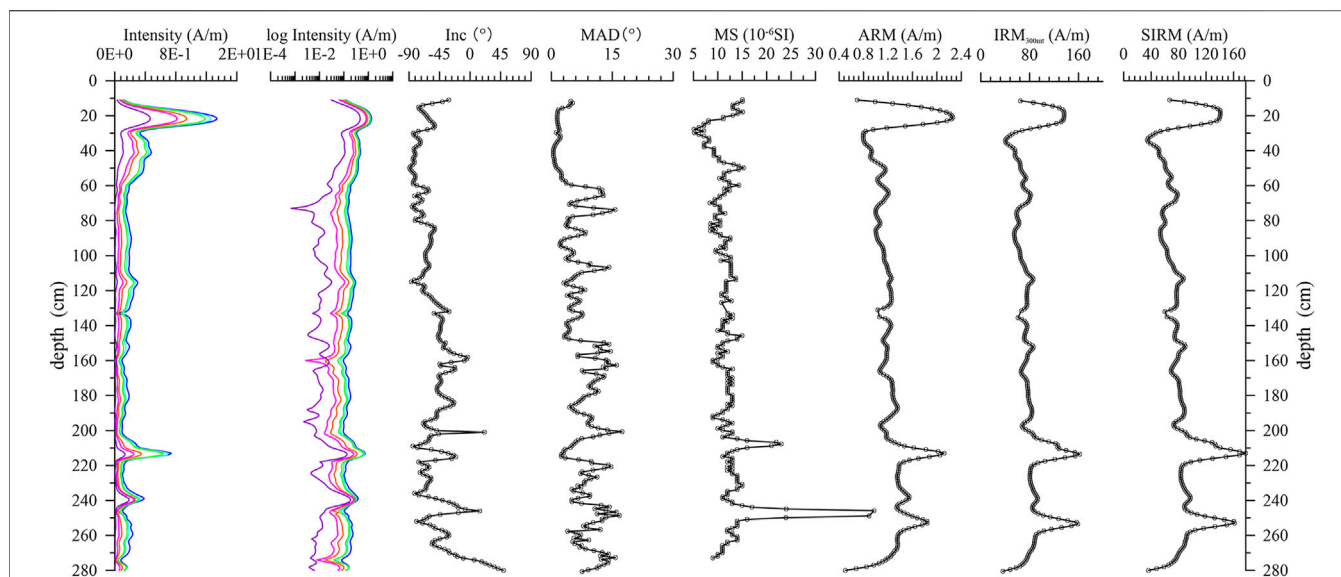
FIGURE 5 | Paleomagnetic results of the core ANT32-RA05C. Intensity, magnetic intensity; log Intensity, logarithmic scale; color lines, NRMs subject to 10, 15, 30, 40, 60, and 80 mT alternating field demagnetization from right to left, respectively; Inc, magnetic inclination; MAD, maximum angle deviation; MS, magnetic susceptibility; ARM, anhysteretic remanent magnetization; IRM, isothermal remanent magnetization; SIRM, saturation isothermal remanent magnetization.
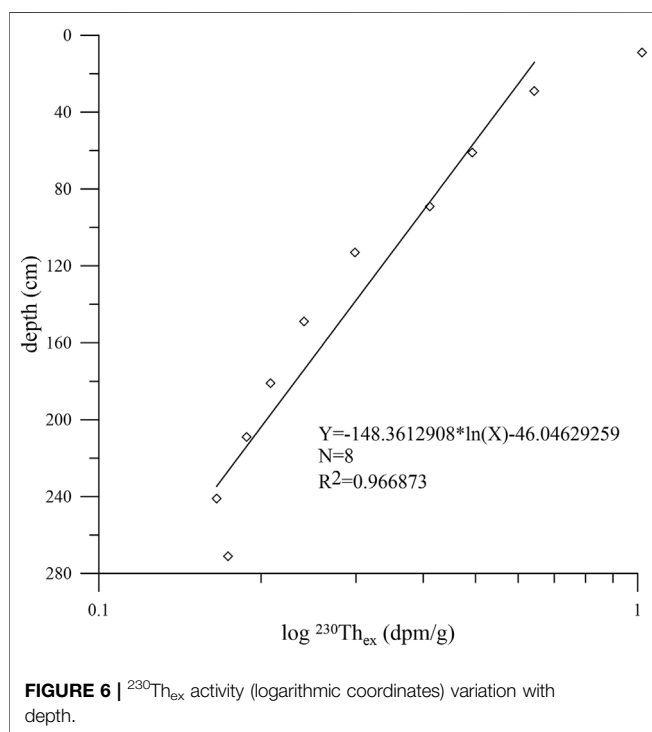

FIGURE 6 | $^{230}Th_{ex}$ activity (logarithmic coordinates) variation with depth.

Analysis, Ocean University of China. The major elements were determined by an inductively coupled plasma–optical emission spectrometry (ICP–OES) Icap6300 at the Key Laboratory of Marine Geology and Metallogeny, First Institute of Oceanography, Ministry of Natural Resources of China, and before the measurement, the samples were dried and ground, and digested by nitric acid and hydrofluoric acid (Bi et al., 2021),

with the standard substance GSD-9 for quality tests. For ^{230}Th dating, the sediments were measured by using a multichannel α-spectrometer OCTETE-PLUS, AMETEK, following the methods listed in Knight et al. (2014) in the Key Laboratory of Cenozoic Geology and Environment, Institute of Geology and Geophysics, Chinese Academy of Sciences.

RESULTS

IRD Changes

Glacial diamictons are broadly found in the sediments across the Ross Sea (Domack et al., 1999), mainly containing terrigenous fine silt and clay, biogenic siliceous materials, and IRDs (Anderson et al., 1984). The sand component (grain-size > 63 μm) is commonly used as an indicator of IRD (Reimnitz et al., 1998; Wang et al., 2009), for which the seasonal sea ice carries relatively finer particles (<250 μm) and large ice chunks and icebergs transport coarser ones (>250 μm) (Darby and Paula, 2008; Phillips and Grantz, 2010). Combining the IRD data and lithological characteristics, the core ANT32-RA05C can be divided into three sections (**Figure 2**) and described as follows.

1) Section-1, above 16 cm in depth. This section is the coarsest layer, rich in sands and gravels. The average IRD (>63 μm and >250 μm) contents are about 44 and 32%, respectively. The maximum diameter of the gravels is ~8 cm found at 3–8 cm in depth. *2)* Section-2, 16–52 cm in depth. The sediments are brownish clay and silt, which are relatively fine, with only 10% IRDs (>63 μm). 3) Section-3, below 52 cm in depth. This section contains olive and gray clay and silt, and the grainsize changes are small. The average IRD (>63 μm and >250 μm) contents are

TABLE 2 | U-Th content and isotope analytical data of the core ANT32-RA05C.

Depth (cm)	$^{234}U/^{238}U$ $\pm2\sigma$	$^{234}U\pm2\sigma$ (dpm/g)	$^{230}Th/^{232}Th$ $\pm2\sigma$	$^{230}Th\pm2\sigma$ (dpm/g)	$^{230}Th_{ex}\pm2\sigma$ (dpm/g)
9	0.8846 ± 0.0023	1.1524 ± 0.0041	1.4254 ± 0.0112	2.1717 ± 0.0173	1.0193 ± 0.0174
29	0.8762 ± 0.0024	0.9338 ± 0.0033	0.9077 ± 0.0103	1.5770 ± 0.0180	0.6432 ± 0.0077
61	0.8856 ± 0.0024	0.8982 ± 0.0030	0.6721 ± 0.0100	1.3917 ± 0.0161	0.4935 ± 0.0059
89	0.8729 ± 0.0024	0.8764 ± 0.0030	0.6725 ± 0.0099	1.2879 ± 0.0160	0.4115 ± 0.0053
113	0.8956 ± 0.0024	0.8909 ± 0.0031	0.7925 ± 0.0101	1.1897 ± 0.0139	0.2987 ± 0.0036
149	0.8941 ± 0.0027	0.9680 ± 0.0039	0.7004 ± 0.0099	1.2084 ± 0.0163	0.2404 ± 0.0034
181	0.8945 ± 0.0026	0.9352 ± 0.0036	0.7374 ± 0.0100	1.1436 ± 0.0150	0.2084 ± 0.0028
209	0.9076 ± 0.0023	0.9875 ± 0.0032	0.8437 ± 0.0100	1.1754 ± 0.0141	0.1880 ± 0.0023
241	0.8974 ± 0.0024	0.9712 ± 0.0033	0.6885 ± 0.0100	1.1365 ± 0.0170	0.1654 ± 0.0025
271	0.9169 ± 0.0023	0.9915 ± 0.0031	0.8081 ± 0.0101	1.1652 ± 0.0146	0.1736 ± 0.0022
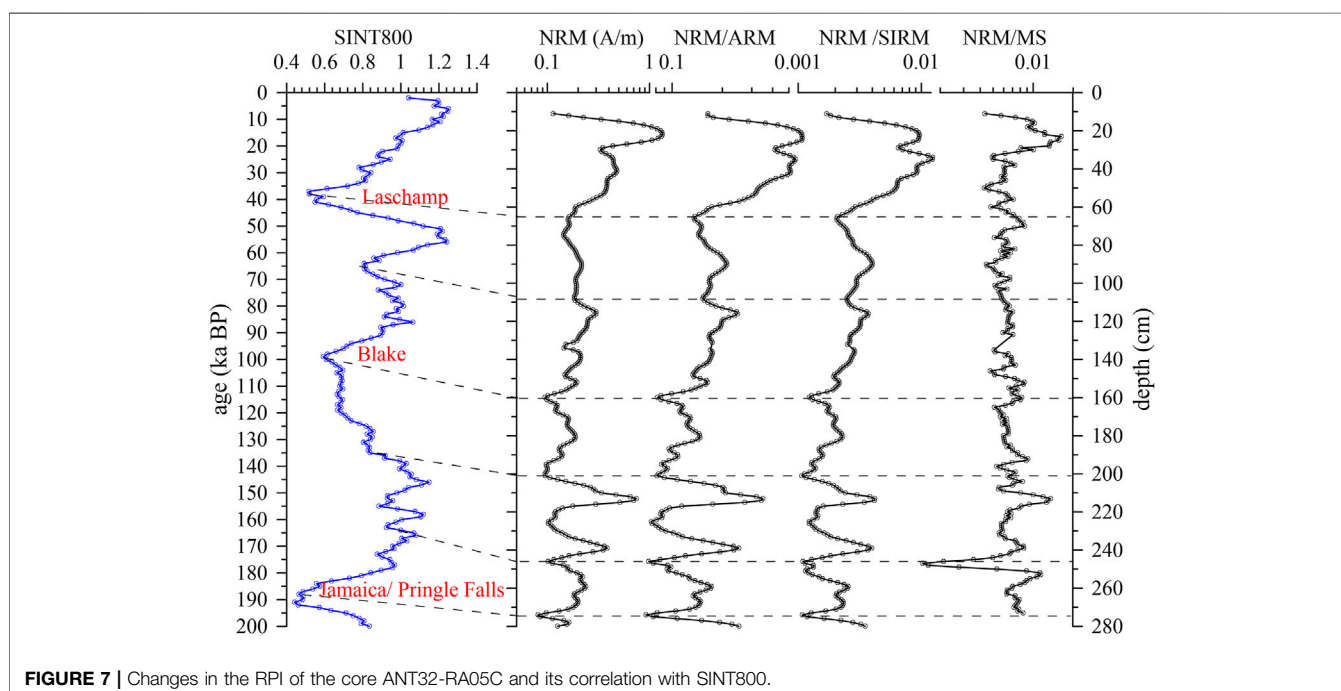
FIGURE 7 | Changes in the RPI of the core ANT32-RA05C and its correlation with SINT800.

about 32 and 19%, respectively, and the diameter of gravels ranges from 0.5 to 4 cm.

Geochemical Characteristics

The chemical composition of 70 sediment samples is determined for the core ANT32-RA05C, and the average content of SiO$_2$ is 66.9%, followed by 11.2% Al$_2$O$_3$ and 4.3% Fe$_2$O$_3$. For stratigraphic changes (**Figure 3**), the SiO$_2$ content is higher in coarse-grained sediments, and Al$_2$O$_3$ and Fe$_2$O$_3$ have an opposite pattern.

There are two main sources of element Si, namely, terrigenous and biogenic sources, and the former is from the quartz debris and clay minerals, while the latter is biogenic, such as diatom frustules and sponge spicules. A correlation analysis can reveal the relationship between the different sources, and as a result (**Table 1**), SiO$_2$ is positively correlated with the IRD, biogenic silica, and CaO but negatively correlated with the rest. The positive relationship between biogenic silica, CaO, and element Si indicates a close relationship between them, likely relating to marine productivity changes. Previous studies show that over 90% of minerals in coarse sediments of the Ross Sea are feldspathic quartz (Li et al., 2021), which are strongly resistant to physical weathering (Cook et al., 2017; Hobbs et al., 2016), as observed in the range of the chemical index of alteration (CIA, 47–67) in the core ANT32-RA05C. Considering the negative relationship between SiO$_2$ and Al$_2$O$_3$, it is inferred that the terrigenous debris with element Si is mainly from quartz.

TABLE 3 | Age model of the core ANT32-RA05C.

Depth (cm)	Age (ka)	Magnetic event
0	0	—
66	36	Laschamp
108	64	—
160	99	Blake
201	134	—
246	163	—
274	191	Jamaica/Pringle Falls

Magnetic Results

Subjected to the alternating field demagnetization, characteristic remanence can be separated between 15 and 60 mT (**Figure 4**), and all the samples obtain reliable results using 4–11 steps with a maximum angular deviation (MAD) of <15°. The remanence intensity of the samples changes little from the bottom to top (**Figure 5**), with three peaks at 236–242 cm, 207–217 cm, and 13–58 cm. The magnetic inclination is mainly reversed, consistent with the geographic location of the core.

The magnetic parameters can reveal the changes in magnetic minerals and/or magnetic domains. For example, ARM is usually sensitive to single-domain (SD) grains (Maher, 1988; Duan et al., 2012), and SIRM can be used to infer magnetic particles excluding the influence of superparamagnetic (SP) grains (Evans and Heller, 2003). Inferred from the magnetic parameters (**Figure 5**), magnetic minerals are concentrated at 236–242 cm, 207–217 cm, and 13–58 cm, consistent with the intervals of high remanence intensity. All these findings suggest a relatively stable process, which can be employed to establish an RPI curve for comparison.

^{230}Th Results

The U and Th isotopes are listed in **Table 2**, in which the values are similar and the ^{230}Th content gradually decreased to the bottom, generally fulfilling the base of ^{230}Th-excess dating (Osmond, 1979; Xia, 1989; Edwards et al., 2003). Assuming that ^{230}Th$_{ex}$ flux is constant over the time of deposition, ^{230}Th$_{ex}$ decays exponentially with the depths, and the slope coefficient of the regression represents the sedimentation rate (Scholten et al., 1994). The calculation is as follows:

$$\ln {}^{230}\text{Th}_{ex(h)} = (-\lambda/k) \times h + \ln {}^{230}\text{Th}_{ex(0)},$$

where ^{230}Th$_{ex\,(h)}$ and ^{230}Th$_{ex\,(0)}$ are the excess radioactivity of ^{230}Th at depth "h" and the surface, respectively. λ is the ^{230}Th decay constant, 9.21738×10^{-6}, and the curve with $-\lambda/V$ indicates the slope. Based on the estimates shown in **Figure 6**, the average sedimentation rate is 1.37 cm/kyr.

DISCUSSION

Establishing the Age Model

Dating sediments in polar seas is much more difficult than that in other areas (Wang et al., 2009), and an integrated result of various dating methods is commonly used. According to an average sedimentation rate of 1.37 cm/kyr from the ^{230}Th method, the bottom age of the core ANT32-RA05C is about 200 ka, offering a preliminary constraint for RPIs.

To refine the age model, RPI is employed, as suggested in previous studies (Sagnotti et al., 2001; Branchfeld et al., 2003; Macrì et al., 2005; Macrì et al., 2006; Collins et al., 2012; Xiao et al.,
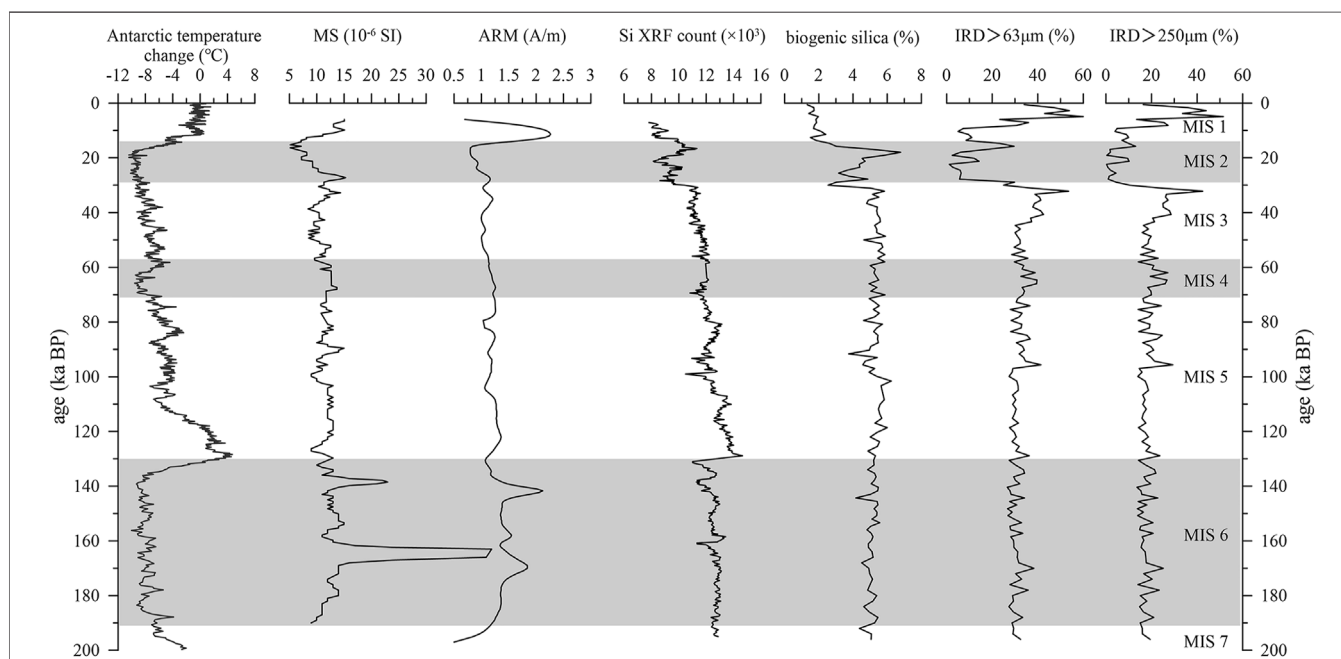

FIGURE 8 | Comparison between the various paleoenvironmental proxies. The Antarctic temperature data are from Jouzel et al. (2007); MIS, marine isotope stage.

2016). However, NRMs are sensitive to changes in magnetic minerals, and to remove this potential influence, various normalizations have been proposed (King et al., 1983; Meynadier et al., 1992; Tauxe, 1993), including MS, ARM, and IRMs. Accordingly, the RPIs of the core ANT32-RA05C can be obtained, and all the curves show a similar pattern (**Figure 7**). Subsequently, the derived RPIs are correlated with the SINT800 RPI curve (Guyodo and Valet, 1999), to obtain additional age controls. Specifically, the low RPI at 274 cm could be correlated with the magnetic excursion of Jamaica/Pringle Falls at ~191 ka (Guyodo and Valet, 1999), and other constraints are listed in **Table 3**. Based on this correlation, there is a high consistency between ANT32-RA05C RPI and SINT800, yielding an average sedimentation rate within 66–274 cm in depth as 1.34 cm/kyr and 1.42 cm/kyr within 66–246 cm in depth. This estimate is close to the ^{230}Th result (1.37 cm/kyr), confirming the reliability of the age model of the studied core in the Ross Sea.

Paleoenvironmental Processes

Based on the age model from ^{230}Th dating and RPI changes, the paleoenvironmental processes in the study area since MIS 7 can be recovered (**Figure 8**). The changes in IRD, biogenic silica, and element Si are selected as the paleoenvironmental proxies, indicating ice-sheet melting and marine productivity, respectively, as aforementioned. For comparison, the temperature reconstruction of the well-studied EDC ice core is displayed for reference (Jouzel et al., 2007). However, because of the little consistency between the magnetic parameters and the Antarctic temperature and other proxies of the core ANT32-RA05C (**Figure 8**), magnetic properties are not included in this discussion.

As shown in **Figure 8**, element Si can be well correlated with the changes in the Antarctic temperature. Specifically, the Si content fluctuated during MIS 6, increased sharply at the MIS 6/5 boundary, decreased slowly during MIS 3, and increased again since ~20 ka. It is then inferred that the marine productivity in the Ross Sea covaried with the Antarctic temperature changes on the glacial-interglacial timescales, agreeing well with the previous studies in Antarctica (Pudsey and Howe, 1998; Diekmann, 2007; Anderson et al., 2009; Xiao et al., 2016). During the LGM, the Antarctic temperature declined to a much low level, and sea ice largely expanded, causing a significant decrease of the IRD transport and thus the fine-grained sediments. However, the regional environment within this key interval may be unstable since all the proxies changed greatly and frequently (**Figure 8**). After the LGM, the Antarctic temperature increased rapidly, icebergs collapsed, and IRD increased. Meanwhile, the warming led to an increase in marine productivity, inferred from biogenic silica content of the core ANT32-RA05C. Moreover, the changes in IRD and biogenic silica are not synchronous, while IRD changes are consistent with element Si, indicating that biogenic processes may precede changes in the ice sheet in the Ross Ice Shelf during the last deglaciation, thus highlighting the role of oceanic circulation in ice-sheet retreat (Hillenbrand et al., 2009; Williams et al., 2019). In the Holocene, the Antarctic temperature rises as high as present, and IRD increased significantly to the highest level (up to 54%) over the past 200 kyr, suggesting that ice sheet, regional temperature, and marine productivity are coupled again as similar in other intervals.

As an important proxy of iceberg drift and ice sheet evolution, IRD has been broadly used in the palaeoceanographic research in the Arctic and Antarctic regions (Darby and Paula, 2008; Wang et al., 2009), representing a climatic transition from cold to warm. In the core ANT32-RA05C, three intervals with evident IRDs are recognized: 29–32 ka, 15–17 ka, and 5 ka to present. However, IRDs did not exactly covary with the temperature changes, such as inconsistent cases in 29–32 ka and MIS6/5 boundary. The difference between the IRDs of the core ANT32-RRA05C and Antarctic temperature might be caused by proxy sensitivity or a different mechanism during climatic transitions. For example, IRD events could be influenced by factors such as ice shelf stability, sea-level changes, regional sedimentary dynamics, sea surface temperature, and shelf topography (Teitler, 2010; Patterson et al., 2014; Li et al., 2021). Considering the similarity of change patterns of the Antarctic temperature between different intervals, it is inferred that the ice shelf stability could be a major reason in the diverse IRD records, which are worthy of further investigation in the future.

CONCLUSION

By studying the sediment core ANT32-RA05C, which was collected from the continental slope of the Ross Sea, the geochronology and paleoenvironmental processes in the study area are documented since the Late Pleistocene. Paleomagnetic and ^{230}Th dating are integrated to establish the age model, and IRD, element Si, and biogenic silica proxies are employed for research on paleoenvironmental changes. Based on these pieces of evidence, our conclusions are as follows.

1) Depending upon ^{230}Th isotopes, the average sedimentation rate is 1.37 cm/kyr, agreeing well with the results (1.34 cm/kyr and 1.42 cm/kyr) of the correlation between the relative paleomagnetic intensity recorded in the core ANT32-RA05C and changes in the Earth's magnetic intensity.
2) IRDs are the major component in the sediments of the studied core in the past 200 kyr, and siliceous deposits are also evident, indicating the influence of marine productivity.
3) Ice-sheet melting and marine productivity in the Ross Sea generally covaried in the Late Pleistocene, while a leading phase of biogenic silica to IRD changes is observed in the last deglaciation.

Combining these findings, a close correlation of regional paleoenvironmental processes to changes in the Antarctic temperature is revealed, inferring that both the IRD input and primary productivity were likely enhanced in a warm climate.

Therefore, it is proposed that the sedimentary records in the Ross Sea document a major role of oceanic circulation in the ice-sheet evolution in the last deglaciation, which is worthy of further investigation.

DATA AVAILABILITY STATEMENT

The original contributions presented in the study are included in the article/Supplementary Materials, further inquiries can be directed to the corresponding authors.

AUTHOR CONTRIBUTIONS

GL, LY and RB designed this study. BH, YL, YJ, YL and LW carried out sample and data analyses. GL and LY primarily wrote the manuscript with input from all other co-authors.

REFERENCES

Anderson, J. B., Brake, C. F., and Myers, N. C. (1984). Sedimentation on the Ross Sea continental Shelf, Antarctica. *Mar. Geology.* 57, 295–333. doi:10.1016/0025-3227(84)90203-2

Anderson, J. B., Conway, H., Bart, P. J., Witus, A. E., Greenwood, S. L., Mckay, R. M., et al. (2014). Ross Sea Paleo-Ice Sheet Drainage and Deglacial History during and since the LGM. *Quat. Sci. Rev.* 100 (17), 31–54. doi:10.1016/j.quascirev.2013.08.020

Anderson, R. F., Ali, S., Bradtmiller, L. I., Nielsen, S. H. H., Fleisher, M. Q., Anderson, B. E., et al. (2009). Wind-Driven Upwelling in the Southern Ocean and the Deglacial Rise in Atmospheric CO 2. *Science* 323, 1443–1448. doi:10.1126/science.1167441

Bart, P. J., and Cone, A. N. (2012). Early Stall of West Antarctic Ice Sheet advance on the Eastern Ross Sea Middle Shelf Followed by Retreat at 27,50014C Yr BP. *Palaeogeogr. Palaeoclimatol. Palaeoecol.* 335-336, 52–60. doi:10.1016/j.palaeo.2011.08.007

Bi, D., Shi, X., Huang, M., Yu, M., Zhou, T., Zhang, Y., et al. (2021). Geochemical and Mineralogical Characteristics of Deep-Sea Sediments from the Western North Pacific Ocean: Constraints on the Enrichment Processes of Rare Earth Elements. *Ore Geology. Rev.* 138, 104318. doi:10.1016/j.oregeorev.2021.104318

Brachfeld, S., Pinzon, J., Darley, J., Sagnotti, L., Kuhn, G., Florindo, F., et al. (2013). Iron Oxide Tracers of Ice Sheet Extent and Sediment Provenance in the ANDRILL AND-1B Drill Core, Ross Sea, Antarctica. *Glob. Planet. Change* 110, 420–433. doi:10.1016/j.gloplacha.2013.09.015

Branchfeld, S., Acton, G. D., Guyodo, Y., and Banerjee, S. K. (2003). High-resolution Paleomagnetic Records from Holocene Sediments from the Palmer Deep, Western Antarctic Peninsula. *Earth Planet. Sci. Lett.* 181, 429–441. doi:10.1016/S0012-821X(00)00211-9

Carter, L., Mccave, I. N., and Williams, M. J. M. (2008). Chapter 4 Circulation and Water Masses of the Southern Ocean: A Review. *Dev. Earth Environ. Sci.* 8, 85–114. doi:10.1016/S1571-9197(08)00004-9

Channell, J. E. T., Xuan, C., and Hodell, D. A. (2009). Stacking Paleointensity and Oxygen Isotope Data for the Last 1.5 Myr (PISO-1500). *Earth Planet. Sci. Lett.* 283, 14–23. doi:10.1016/j.epsl.2009.03.012

Collins, L. G., Hounslow, M. W., Allen, C. S., Hodgson, D. A., Pike, J., and Karloukovski, V. V. (2012). Palaeomagnetic and Biostratigraphic Dating of marine Sediments from the Scotia Sea, Antarctica: First Identification of the Laschamp Excursion in the Southern Ocean. *Quat. Geochronol.* 7, 67–75. doi:10.1016/j.quageo.2011.10.002

Cook, C. P., Hemming, S. R., van de Flierdt, T., Pierce Davis, E. L., Williams, T., Galindo, A. L., et al. (2017). Glacial Erosion of East Antarctica in the Pliocene: A Comparative Study of Multiple marine Sediment Provenance Tracers. *Chem. Geology.* 466, 199–218. doi:10.1016/j.chemgeo.2017.06.011

Darby, D. A., and Zimmerman, P. (2008). Ice-rafted Detritus Events in the Arctic during the Last Glacial Interval, and the Timing of the Innuitian and Laurentide Ice Sheet Calving Events. *Polar Res.* 27 (2), 114–127. doi:10.1111/j.1751-8369.2008.00057.x

Diekmann, B. (2007). Sedimentary Patterns in the Late Quaternary Southern Ocean. *Deep Sea Res. Part Topical Stud. Oceanography* 54, 2350–2366. doi:10.1016/j.dsr2.2007.07.025

Domack, E. W., Jacobson, E. A., Shipp, S., and Anderson, J. B. (1999). Late Pleistocene-Holocene Retreat of the West Antarctic Ice Sheet in the Ross Sea: Part 2 – Sedimentologic and Stratigraphic Signature. *Geol. Soc. America Bull.* 111 (10), 1517–1536. doi:10.1130/0016-7606(1999)111<1517:lphrot>2.3.co;2

Dotto, T. S., Naveira Garabato, A., Bacon, S., Tsamados, M., Holland, P. R., Hooley, J., et al. (2018). Variability of the Ross Gyre, Southern Ocean: Drivers and Responses Revealed by Satellite Altimetry. *Geophys. Res. Lett.* 45, 6195–6204. doi:10.1029/2018GL078607

Duan, Z., Gao, X., and Liu, Q. (2012). Anhysteretic Remanent Magnetization (ARM) and its Application to Geoscience. *Prog. Geophys.* 27 (5), 1929–1938. doi:10.1007/s11783-011-0280-z

Edwards, R. L., Gallup, C. D., and Cheng, H. (2003). Uranium-series Dating of marine and Lacustrine Carbonates. *Rev. Mineralogy Geochem.* 52, 363–405. doi:10.2113/0520363

Evans, M. E., and Heller, F. (2003). *Environmental Magnetism: Principles and Applications of Enviromagnetics*. New York: Academic Press.

Guyodo, Y., and Valet, J.-P. (1999). Global Changes in Intensity of the Earth's Magnetic Field during the Past 800 Kyr. *Nature* 399, 249–252. doi:10.1038/20420

Hillenbrand, C.-D., Kuhn, G., and Frederichs, T. (2009). Record of a Mid-pleistocene Depositional Anomaly in West Antarctic continental Margin Sediments: an Indicator for Ice-Sheet Collapse? *Quat. Sci. Rev.* 28, 1147–1159. doi:10.1016/j.quascirev.2008.12.010

Hobbs, W. R., Massom, R., Stammerjohn, S., Reid, P., Williams, G., and Meier, W. (2016). A Review of Recent Changes in Southern Ocean Sea Ice, Their Drivers and Forcings. *Glob. Planet. Change* 143, 228–250. doi:10.1016/j.gloplacha.2016.06.008

Jouzel, J., Masson-Delmotte, V., Cattani, O., Dreyfus, G., Falourd, S., Hoffmann, G., et al. (2007). Orbital and Millennial Antarctic Climate Variability over the Past 800,000 Years. *Science* 317, 793–796. doi:10.1126/science.1141038

Jovane, L., Acton, G., Florindo, F., and Verosub, K. (2008). Geomagnetic Field Behavior at High Latitudes from a Paleomagnetic Record from Eltanin Core 27-21 in the Ross Sea Sector, Antarctica. *Earth Planet. Sci. Lett.* 267, 435–443. doi:10.1016/j.epsl.2007.12.006

King, J. W., Banerjee, S. K., and Marvin, J. (1983). A New Rock-Magnetic Approach to Selecting Sediments for Geomagnetic Paleointensity Studies: Application to Paleointensity for the Last 4000 Years. *J. Geophys. Res.* 88 (7), 5911–5921. doi:10.1029/JB088iB07p05911

Knight, A. W., Eitrheim, E. S., Nelson, A. W., Nelson, S., and Schultz, M. K. (2014). A Simple-Rapid Method to Separate Uranium, Thorium, and Protactinium for U-Series Age-Dating of Materials. *J. Environ. Radioactivity* 134, 66–74. doi:10.1016/j.jenvrad.2014.02.010

Li, Y. B., Wang, R. J., Wu, L., and Xiao, W. S. (2021). Glacial Dynamics Evolutions Revealed by Ice-Rafted Debris Record from the Ross Sea Sector of the Southern Ocean since Late Pleistocene (In Chinese with English Abstract). *Quat. Sci.* 41 (3), 662–677. doi:10.11928/j.issn.1001-7410.2021.03.04

Lisé-Pronovost, A., St-Onge, G., Gogorza, C., Haberzettl, T., Preda, M., Kliem, P., et al. (2013). High-resolution Paleomagnetic Secular Variations and Relative Paleointensity since the Late Pleistocene in Southern South America. *Quat. Sci. Rev.* 71, 91–108. doi:10.1016/j.quascirev.2012.05.012

Macrì, P., Sagnotti, L., Dinarès-Turell, J., and Caburlotto, A. (2005). A Composite Record of Late Pleistocene Relative Geomagnetic Paleointensity from the Wilkes Land Basin (Antarctica). *Phys. Earth Planet. Interiors* 151, 223–242. doi:10.1016/j.pepi.2005.03.004

Macrì, P., Sagnotti, L., Lucchi, R. G., and Rebesco, M. (2006). A Stacked Record of Relative Geomagnetic Paleointensity for the Past 270 Kyr from the Western continental Rise of the Antarctic Peninsula. *Earth Planet. Sci. Lett.* 252, 162–179. doi:10.1016/j.epsl.2006.09.037

Maher, B. A. (1988). Magnetic Properties of Some Synthetic Sub-micron Magnetites. *Geophys. J. Int.* 94 (1), 83–96. doi:10.1111/j.1365-246X.1988.tb03429.x

Mckay, R. M., Dunbar, G. B., Naish, T. R., Barrett, P. J., Carter, L., and Harper, M. (2008). Retreat History of the Ross Ice Sheet (Shelf) since the Last Glacial Maximum from Deep-basin Sediment Cores Around Ross Island. *Palaeogeogr. Palaeoclimatol. Palaeoecol.* 260 (1-2), 245–261. doi:10.1016/j.palaeo.2007.08.015

Meynadier, L., Valet, J.-P., Weeks, R., Shackleton, N. J., and Hagee, V. L. (1992). Relative Geomagnetic Intensity of the Field during the Last 140 Ka. *Earth Planet. Sci. Lett.* 114, 39–57. doi:10.1016/0012-821X(92)90150-T

Mosola, A. B., and Anderson, J. B. (2006). Expansion and Rapid Retreat of the West Antarctic Ice Sheet in Eastern Ross Sea: Possible Consequence of Over-extended Ice Streams? *Quat. Sci. Rev.* 25 (17-18), 2177–2196. doi:10.1016/j.quascirev.2005.12.013

Naish, T., Powell, R., Levy, R., Wilson, G., Scherer, R., Talarico, F., et al. (2009). Obliquity-paced Pliocene West Antarctic Ice Sheet Oscillations. *Nature* 458, 322–328. doi:10.1038/nature07867

Ohneiser, C., Yoo, K.-C., Albot, O. B., Cortese, G., Riesselman, C., Lee, J. I., et al. (2019). Magneto-biostratigraphic Age Models for Pleistocene Sedimentary Records from the Ross Sea. *Glob. Planet. Change* 176, 36–49. doi:10.1016/j.gloplacha.2019.02.013

Osmond, J. K. (1979). Accumulation Models of 230Th and 231Pa in Deep Sea Sediments. *Earth-Science Rev.* 15 (2), 95–150. doi:10.1016/0012-8252(79)90024-2

Patterson, M. O., McKay, R., McKay, R., Naish, T., Escutia, C., Jimenez-Espejo, F. J., et al. (2014). Orbital Forcing of the East Antarctic Ice Sheet during the Pliocene and Early Pleistocene. *Nat. Geosci* 7, 841–847. doi:10.1038/ngeo2273

Phillips, R. L., and Grantz, A. (2010). Regional Variations in Provenance and Abundance of Ice-Rafted Clasts in Arctic Ocean Sediments: Implications for the Configuration of Late Quaternary Oceanic and Atmospheric Circulation in the Arctic. *Mar. Geology.* 172, 91–115. doi:10.1016/S0025-3227(00)00101-8

Pudsey, C. J., and Howe, J. A. (1998). Quaternary History of the Antarctic Circumpolar Current: Evidence from the Scotia Sea. *Mar. Geology.* 148, 83–112. doi:10.1016/S0025-3227(98)00014-0

Pugh, R. S., McCave, I. N., Hillenbrand, C.-D., and Kuhn, G. (2009). Circum-Antarctic Age Modelling of Quaternary marine Cores under the Antarctic Circumpolar Current: Ice-Core Dust-Magnetic Correlation. *Earth Planet. Sci. Lett.* 284, 113–123. doi:10.1016/j.epsl.2009.04.016

Reimnitz, E., Mccormick, M., Bischof, J., and Darby, D. A. (1998). Comparing Sea-Ice Sediment Load with Beaufort Sea Shelf Deposits; Is Entrainment Selective? *J. Sediment. Res.* 68 (5), 777–787. doi:10.2110/jsr.68.777

Rignot, E., Jacobs, S., Mouginot, J., and Scheuchl, B. (2013). Ice-shelf Melting Around Antarctica. *Science* 341 (6143), 266–270. doi:10.1126/science.1235798

Sagnotti, L., Macrì, P., Camerlenghi, A., and Rebesco, M. (2001). Environmental Magnetism of Antarctic Late Pleistocene Sediments and Interhemispheric

Correlation of Climatic Events. *Earth Planet. Sci. Lett.* 192, 65–80. doi:10.1016/S0012-821X(01)00438-1

Scholten, J. C., Botz, R., Paetsch, H., Stoffers, P., and Weinelt, M. (1994). High-resolution Uranium-Series Dating of Norwegian-Greenland Sea Sediments: ^{230}Th vs. δ^{18}O Stratigraphy. *Mar. Geology.* 121 (1-2), 77–85. doi:10.1016/0025-3227(94)90158-9

Ship, S., Anderson, J., and Domack, E. (1999). Late Pleistocene-Holocene Retreat of the West Antarctic Ice-Sheet System in the Ross Sea: Part 1. *Geol. Soc. America Bull.* 111 (10), 1486–1516. doi:10.1130/0016-7606(1999)111<1486:lphrot>2.3.co;2

Sikes, E. L., Samson, C. R., Guilderson, T. P., and Howard, W. R. (2000). Old Radiocarbon Ages in the Southwest Pacific Ocean during the Last Glacial Period and Deglaciation. *Nature* 405, 555–559. doi:10.1038/35014581

Skinner, L. C., Fallon, S., Waelbroeck, C., Michel, E., and Barker, S. (2010). Ventilation of the Deep Southern Ocean and Deglacial CO_2 Rise. *Science* 328, 1147–1151. doi:10.1126/science.1183627

Smith, W. O., Jr., Sedwick, P. N., Arrigo, K. R., Ainley, D. G., and Orsi, A. H. (2012). The Ross Sea in a Sea of Change. *Oceanography* 25 (3), 1977–1981. doi:10.1021/es00024a60010.5670/oceanog.2012.80

Stoner, J. S., Laj, C., Channell, J. E. T., and Kissel, C. (2002). South Atlantic and North Atlantic Geomagnetic Paleointensity Stacks (0-80ka): Implications for Inter-hemispheric Correlation. *Quat. Sci. Rev.* 21 (10), 1141–1151. doi:10.1016/S0277-3791(01)00136-6

Tauxe, L. (1993). Sedimentary Records of Relative Paleointensity of the Geomagnetic Field: Theory and Practice. *Rev. Geophys.* 31, 319–354. doi:10.1029/93RG01771

Teitler, L., Warnke, D. A., Venz, K. A., Hodell, D. A., Becquey, S., Gersonde, R., et al. (2010). Determination of Antarctic Ice Sheet Stability over the Last ~500 Ka through a Study of Iceberg-Rafted Debris. *Paleoceanography* 25, PA1202. doi:10.1029/2008PA001691

Wang, R., Xiao, W., Li, W., and Sun, Y. (2009). Late Quaternary Ice-Rafted Detritus Events in the Chukchi Basin, Western Arctic Ocean. *Chin. Sci. Bull.* 55 (23), 432–440. doi:10.1007/s11434-009-0424-8

Williams, T. J., Hillenbrand, C. D., Piotrowski, A. M., Allen, C. S., Frederichs, T., Smith, J. A., et al. (2019). Paleocirculation and Ventilation History of Southern Ocean Sourced Deep Water Masses during the Last 800,000 Years. *Paleoceanography and Paleoclimatology* 34, 833–852. doi:10.1029/2018PA003472

Wilson, G. S., Levy, R. H., Naish, T. R., Powell, R. D., Florindo, F., Ohneiser, C., et al. (2012). Neogene Tectonic and Climatic Evolution of the Western Ross Sea, Antarctica - Chronology of Events from the AND-1B Drill Hole. *Glob. Planet. Change* 96-97, 189–203. doi:10.1016/j.gloplacha.2012.05.019

Xia, M. (1989). *U-series Dating Method and Laboratory Technology*. Lanzhou: Lanzhou University Press. (In Chinese).

Xiao, W., Frederichs, T., Gersonde, R., Kuhn, G., Esper, O., and Zhang, X. (2016). Constraining the Dating of Late Quaternary marine Sediment Records from the Scotia Sea (Southern Ocean). *Quat. Geochronol.* 31, 97–118. doi:10.1016/j.quageo.2015.11.003

Yokoyama, Y., Anderson, J. B., Yamane, M., Simkins, L. M., Miyairi, Y., Yamazaki, T., et al. (2016). Widespread Collapse of the Ross Ice Shelf during the Late Holocene. *Proc. Natl. Acad. Sci. U.S.A.* 113 (9), 2354–2359. doi:10.1073/pnas.1516908113

Conflict of Interest: The authors declare that the research was conducted in the absence of any commercial or financial relationships that could be construed as a potential conflict of interest.

Publisher's Note: All claims expressed in this article are solely those of the authors and do not necessarily represent those of their affiliated organizations, or those of the publisher, the editors, and the reviewers. Any product that may be evaluated in this article, or claim that may be made by its manufacturer, is not guaranteed or endorsed by the publisher.